ORGANOMETALLICS
Article

*Organometallics* **2009,** *28,* 4945–4957 4945
DOI: 10.1021/om900231c

# Crucial Role of the Amidine Moiety in Methylenamino Phosphine-Type Ligands for the Synthesis of Tethered $\eta^6$-Arene-$\eta^1$-*P* Ruthenium(II) Complexes: Experimental and Theoretical Studies

Damien Arquier,[†] Laure Vendier,[†] Karinne Miqueu,[‡] Jean-Marc Sotiropoulos,[‡] Stéphanie Bastin,[†] and Alain Igau*[,†]

[†]*CNRS, LCC (Laboratoire de Chimie de Coordination), 205 Route de Narbonne, F-31077 Toulouse, France, and Université de Toulouse, UPS, INPT, LCC, F-31077 Toulouse, France, and* [‡]*Institut Pluridisciplinaire de Recherche sur l'Environnement et les Matériaux (IPREM), UMR CNRS 5254, Equipe Chimie-Physique, Université de Pau et des Pays de l'Adour, Hélioparc, 2 Avenue du Président Angot, 64053 Pau Cedex 09, France*

*Received March 26, 2009*

Methyleneaminophosphine ligands R′C(Ph)=N−$PPh_2$ (R′ = H (**1**), Ph (**4**)) are unable to form tethered $\eta^6$-arene-$\eta^1$-*P* ruthenium(II) complexes **3** and **6** starting from their corresponding $\eta^1$-*P* metallic precursors **2** and **5**. In marked contrast, straightforward high-yield synthesis of tethered $\eta^6$-arene-$\eta^1$-*P* ruthenium(II) complexes **9a**,**b** was achieved upon addition of methylenaminophosphine-type ligands *i*-$Pr_2$N−C(Ph)=N−$PR_2$ **7** (R = Ph (**a**), *i*-Pr (**b**)) on the ruthenium precursor [(*p*-cymene)$RuCl_2$]$_2$ at 80 °C. We have observed by X-ray crystallographic analyses the unprecedented structural adaptive behavior of the *N*-phosphino amidine ligands **7a**,**b** upon the untethered $\eta^1$-*P* **8a**,**b** or tethered $\eta^6$-arene-$\eta^1$-*P* **9a**,**b** coordination mode in ruthenium(II) complexes. The imino nitrogen atom of the amidine moiety in **7a**,**b** behaves as a "universal joint". In order to minimize the steric hindrance in the second coordination sphere of complexes **8a**,**b**, the value of the C1−N1−P1 bond angle of the amidine moiety widened from 119−122° in **7a**,**b** to 133°, which corresponds to a dramatic change in the geometry of the *N*-phosphino amidine ligands. Moreover, in order to reduce the strain induced by the tethered coordination mode, the value of the C1−N1−P1 bond angle in the amidine moiety in ruthenium(II) complexes **9a**,**b** decreases to 116°. DFT calculations have been carried out in order to gain more insight into the structural and electronic properties of the methylenaminophosphine ligands R′-C(Ph)=N-$PPh_2$ as well as the tethered and untethered ruthenium complexes. Moreover, the reaction feasability has also been theoretically discussed.

## Introduction

Arene ruthenium(II) half-sandwich complexes **I** (Figure 1) have been intensively investigated over the past decades[1] and appear to be very useful catalysts or catalyst precursors for a wide range of reactions such as alkene hydrogenation,[2] Diels−Alder reactions,[3] enantioselective transfer hydrogenation of ketones and imines,[4] alkene metathesis,[5] and cyclopropanation,[6] to name a few.

It is well established that arene ruthenium(II) complexes **I** are prone to arene substitution[7] and can undergo loss of the arene ligand during the catalytic cycle. In some cases, this loss is unwanted and may be detrimental to the catalyst activity. In an attempt to improve the stability of such complexes and to increase stereocontrol at the metal center of chiral catalysts, particular attention has been devoted to development of arene-tethered ruthenium(II) complexes **II**, incorporating an $\eta^6$-arene-$\eta^1$-*L*-donor atom ligand (Figure 1).[8]

*To whom correspondence should be addressed: E-mail: alain.igau@lcc-toulouse.fr.

(1) (a) Therrien, B. *Coord. Chem. Rev.* **2009**, *253*, 493. (b) Le Bozec, H.; Touchard, D.; Dixneuf, P. H. *Adv. Organomet. Chem.* **1989**, *29*, 163. (c) Bennett, M. A. *Coord. Chem. Rev.* **1997**, *166*, 225.

(2) (a) Bhalla, R.; Boxwell, C. J.; Duckett, S. B.; Dyson, P. J.; Humphrey, D. G.; Steed, J. W.; Suman, P. *Organometallics* **2002**, *21*, 924. (b) Cesarotti, E.; Rimoldi, I.; Spalluto, P.; Demartin, F. *Tetrahedron: Asymmetry* **2007**, *18*, 1278. (c) Daguenet, C.; Scopelliti, R.; Dyson, P. J. *Organometallics* **2004**, *23*, 4849. (d) Chaplin, A. B.; Dyson, P. J. *Organometallics* **2007**, *26*, 2447.

(3) (a) Faller, J. W.; Grimmond, B. J.; D'Alliessi, D. G. *J. Am. Chem. Soc.* **2001**, *123*, 2525. (b) Carmona, D.; Vega, C.; Garcá, N.; Lahoz, F. J.; Elipe, S.; Oro, L. A.; Pilar Lamata, M.; Viguri, F.; Borao, R. *Organometallics* **2006**, *25*, 1592. (c) Davies, D. L.; Fawcett, J.; Garratt, S. A.; Russell, D. R. *Organometallics* **2001**, *20*, 3029.

(4) (a) Hashiguchi, S; Fujii, A.; Takehara, J.; Ikariya, T.; Noyori, R. *J. Am. Chem. Soc.* **1995**, *117*, 7562. (b) Uematsu, N.; Fujii, A.; Hashiguchi, S; Ikariya, T.; Noyori, R. *J. Am. Chem. Soc.* **1996**, *118*, 4916. (c) Noyori, R.; Hashiguchi, S. *Acc. Chem. Res.* **1997**, *30*, 97. (d) Palmer, M. J.; Wills, M. *Tetrahedron: Asymmetry* **1999**, *10*, 2045. (e) Gladiali, S.; Alberico, E. *Chem. Soc. Rev.* **2006**, *35*, 226.

(5) (a) Fürstner, A.; Picquet, M.; Bruneau, C.; Dixneuf, P. H. *Chem. Commun.* **1998**, 1315. (b) Jafarpour, L.; Huang, J.; Stevens, E. D.; Nolan, S. P. *Organometallics* **1999**, *18*, 3760. (c) Castarlenas, R.; Vovard, C.; Fischmeister, C.; Dixneuf, P. H. *J. Am. Chem. Soc.* **2006**, *128*, 4079.

(6) (a) Huber, D.; Kumar, P. G. A.; Pregosin, P. S.; Mezzetti, A. *Organometallics* **2005**, *24*, 5221. (b) Huber, D.; Mezzetti, A. *Tetrahedron: Asymmetry* **2004**, *15*, 2193. (c) Nishiyama, H.; Soeda, N.; Naito, T.; Motoyama, Y. *Tetrahedron: Asymmetry* **1998**, *9*, 2865.

(7) Bennett, M. A.; Smith, A. K. *J. Chem. Soc., Dalton Trans.* **1974**, 233.

(8) (a) Morris, D. J.; Hayes, A. M.; Wills, M. *J. Org. Chem.* **2006**, *71*, 7035. (b) Faller, J. W.; Fontaine, P. P. *Organometallics* **2005**, *24*, 4132. (c) Umezawa-Vizzini, K.; Guzman-Jimenez, I. Y.; Whitmire, K. H.; Lee, T. R. *Organometallics* **2003**, *22*, 3059. (d) Çetinkaya, B.; Demir, S.; Ozdemir, I.; Toupet, L.; Sémeril, D.; Bruneau, C.; Dixneuf, P. H. *Chem.—Eur. J.* **2003**, *9*, 2323.



Published on Web 08/03/2009

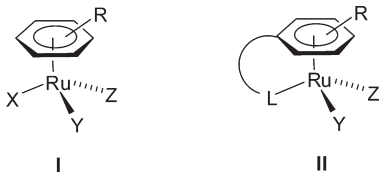


**Figure 1**

Their enhanced robustness toward arene displacement has been evidenced by thermogravimetry[9] and electrochemistry.[10] They have proved to be better catalysts in some reactions than their untethered variants.[8a,11]

We report herein the straightforward synthesis of $\eta^1$-*P* ruthenium(II) complexes incorporating methylenaminophosphine-type ligands R′C(Ph)=N−$PR_2$ (R′=H, Ph, *i*-$Pr_2N$).[12] We experimentally and theoretically demonstrate the superiority of the amidine over the aldimine and imine moieties in methylenaminophosphine-type ligands for the preparation of arene-tethered ruthenium(II) complexes in which the $\eta^6$-coordinated ring is linked to a pendant phosphino group via an imino N=C bridge. All the compounds described herein have been fully characterized by mass spectroscopy, IR, $^{31}P$, $^1H$, and $^{13}C$ NMR, and single-crystal X-ray diffraction studies for **2**, **5**, **7a**,**b**, **8a**,**b**, **9a**,**b**, and **11**. These studies reveal the unprecendented "adaptive" behavior of the *N*-phosphino amidine (phosam) ligands *i*-$Pr_2N$−C(Ph)=N−$PR_2$ upon coordination to ruthenium(II).

## Results and Discussion

$\eta^1$-*P* ruthenium(II) complexes incorporating *N*-phosphino aldimine **2** and *N*-phosphino imine **5** ligands were prepared in 90% and 95% isolated yield, respectively, from the corresponding methylenaminophosphine ligands **1**[13] and **4**[12] and the ruthenium precursor [(*p*-cymene)$RuCl_2]_2$. The phosphorus atom of the methylenaminophosphine ligands **1** and **4** is coordinated to the metal fragment [(*p*-cymene)$RuCl_2$]. The X-ray study revealed an *E*-aldimine stereoisomer for the $\eta^1$-*P* ruthenium(II) complex **2**, as depicted in Figure 2. The aldimine moiety angle C1−N1−P1 is close to 120°, standard for an $sp^2$ nitrogen, and the C1−N1 and N1−P1 bond lengths indicate multiple-bond character (Table 1).

The structure of the corresponding $\eta^1$-*P* ruthenium(II) complex **5** with the methylenaminophosphine **4** has a similar ligand geometry, except for the C1−N1−P1 angle, which is widened to 135.24(19)°. This may be associated with the increased steric hindrance in the second coordination sphere due to the presence of the second phenyl substituent attached to the methylene carbon atom in ligand **4**. Increasing the bond angle around the imino nitrogen atom N1 in **5** avoids the steric interactions between the isopropyl fragment of the *p*-cymene arene ligand and the $=CPh_2$ moiety, which is, therefore, pushed away from the metal center.

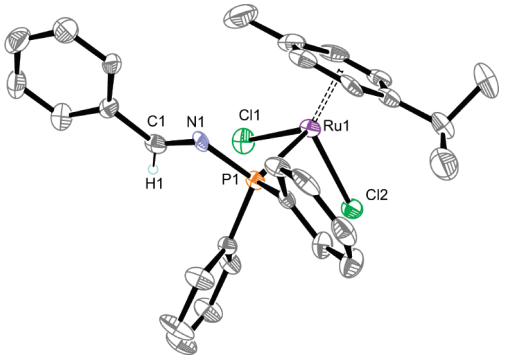


**Figure 2.** Molecular structure of $\eta^1$-*P* methylenaminophosphine ruthenium complex **2**.

**Table 1. Selected Bond Lengths (Å) and Angles (deg) for $\eta^1$-*P* Methylenaminophosphine Ruthenium(II) Complexes 2 and 5**

| | 2 | 5 |
|---|---|---|
| C1−C2 | 1.224(6) | 1.358(6) |
| C1−N1 | 1.280(8) | 1.283(3) |
| N1−P1 | 1.696(5) | 1.678(2) |
| Ru1−P1 | 2.3068(17) | 2.3409(6) |
| N1−C1−C2 | 122.4(6) | 126.4(2) |
| C1−N1−P1 | 121.5(5) | 135.24(19) |
| N1−P1−Ru1 | 108.36(18) | 107.09(7) |
| P1−Ru1−C*[a] | 128.29 | 127.72 |

[a] C* = centroid.

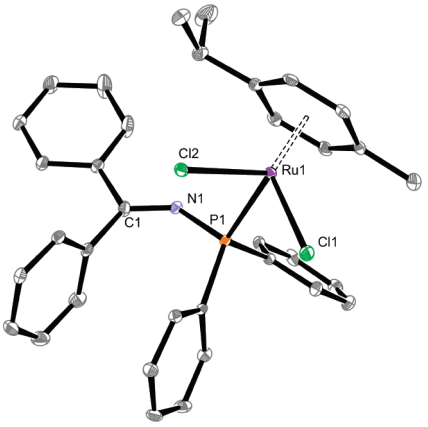


**Figure 3.** Molecular structure of $\eta^1$-*P* methylenaminophosphine ruthenium complex **5**.

Starting from **2** and **5**, the next step was to exchange the *p*-cymene ligand and to form the corresponding tethered products. When **2** was heated at 50 °C for 72 h, it was fully recovered. However, at 80 °C the solution turned immediatly black and the $^{31}P$ NMR spectrum showed a multitude of signals in the range 20 to 177 ppm. No single phosphorus-containing species could be isolated from the reaction mixture. Complex **5** was heated overnight at 80 °C to give, by $^{31}P$ NMR, along with some remaining starting material, an intense signal at 112 ppm and three other minor products at 127, 113, and 47 ppm. By $^1H$ NMR, the chemical shifts observed in the region of 5−6 ppm may correspond to arene-tethered protons. By $^{31}P$ NMR, after 3 days at 80 °C, the signal corresponding to **5** totally vanished and three major phosphorus chemical shifts were detected at 132, 112, and

(9) Simal, F.; Jan, D.; Demonceau, A.; Noels, A. F. *Tetrahedron Lett.* **1999**, *40*, 1653.
(10) (a) Bennett, M. A.; Edwards, A. J.; Harper, J. R.; Khimyak, T.; Willis, A. C. *J. Organomet. Chem.* **2001**, *629*, 7. (b) Smith, P. D.; Wright, A. H. *J. Organomet. Chem.* **1998**, *559*, 141.
(11) (a) Hayes, A. M.; Morris, D. J.; Clarkson, G. J.; Wills, M. *J. Am. Chem. Soc.* **2005**, *127*, 7318. (b) Cheung, F. K.; Hayes, A. M.; Hannedouche, J.; Yim, A. S. Y.; Wills, M. *J. Org. Chem.* **2005**, *70*, 3188. (c) Miyaki, Y.; Onishi, T.; Ogoshi, S.; Kurosawa, H. *J. Organomet. Chem.* **2000**, *616*, 135.
(12) Derivatives of the general structure R′R″C=N−$PR_2$ have been prepared and named for the first time as "methylenaminophosphines" by Schmidpeter and Zeiss; we have used this denomination throughout this paper. Schmidpeter, A.; Zeiss, W. *Chem. Ber.* **1971**, *104*, 1199.
(13) Reed, R. W. Ph.D. Thesis, University of Alberta, **1992**.

**Scheme 1**

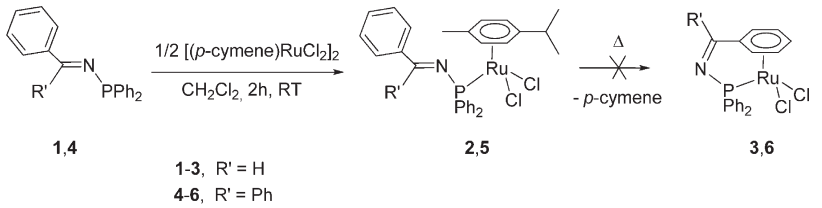


**Table 2. Selected Bond Lengths (Å) and Angles (deg) for Amidine Compounds 7a,b and the Ruthenium Complexes 8a,b, 9a,b, and 11**

| | 7a | 8a | 11 | 9a | 7b | 8b | 9b |
|---|---|---|---|---|---|---|---|
| N2−C1 | 1.363(4) | 1.358(6) | 1.331(4) | 1.326(12) | 1.361(2) | 1.375(3) | 1.340(4) |
| C1−N1 | 1.307(4) | 1.296(6) | 1.299(4) | 1.307(11) | 1.291(2) | 1.295(4) | 1.309(4) |
| N1−P1 | 1.710(3) | 1.654(4) | 1.673(2) | 1.693(8) | 1.7130(16) | 1.672(2) | 1.688(3) |
| Ru1−P1 | | 2.3518(13) | 2.3363(8) | 2.320(3) | | 2.3967(7) | 2.3339(10) |
| N1−C1−N2 | 120.5(3) | 120.1(4) | 123.9(3) | 122.1(8) | 120.08(17) | 119.7(2) | 123.2(3) |
| C1−N1−P1 | 119.2(2) | 132.7(3) | 118.5(2) | 115.6(7) | 121.99(13) | 133.23(19) | 116.4(3) |
| N1−P1−Ru1 | | 112.81(14) | 117.52(9) | 107.8(3) | | 110.66(8) | 106.78(11) |
| P1−Ru1−C*[a] | | 127.99 | 129.08 | 119.42 | | 129.35 | 120.15 |

[a] C* = centroid.

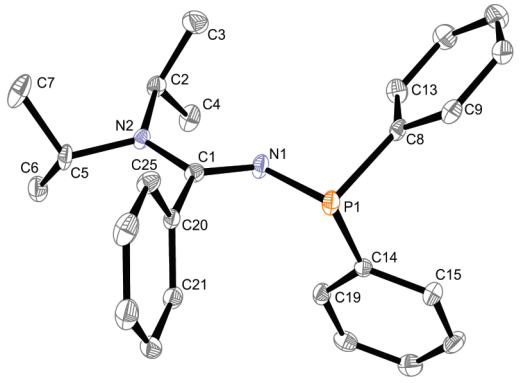


**Figure 4.** Molecular structure of *N*-phosphino amidine ligand **7a**.

**Scheme 2**

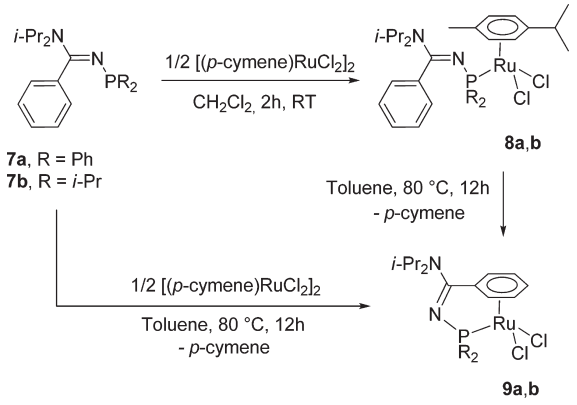


72 ppm, but we were not able to separate and characterize the different reaction products. Therefore, starting from the corresponding $\eta^1$-*P* ruthenium(II) complexes **2** and **5**, methylenaminophosphines R′C(Ph)=N−$PPh_2$ (R′ = H (**1**), Ph (**4**)) are not the appropriate ligands to form the corresponding tethered $\eta^6$-arene-$\eta^1$-*P* ruthenium(II) complexes **3** and **6**.

We then reacted with the ruthenium precursor [(*p*-cymene)$RuCl_2$]$_2$ another class of methylenaminophosphine-type ligands, the *N*-phosphino amidine derivatives of the general form $R'_2N$−C(Ph)=N−$PR_2$. It is noteworthy that very few examples of complexes with *N*-phosphino amidines as ligands have been reported in the literature before our studies.[14] Phosam **7a**[15] was prepared in 82% isolated yield (Figure 4, Table 2).

As expected, the X-ray structure analysis revealed an *E*-stereoisomer for **7a**. The phosphorus atom exhibits a trigonal geometry with a N1−P1 bond distance of 1.710(3) Å, and the amino nitrogen atom *i*-$Pr_2N$− is planar. The significant difference of 0.056 Å between the C1−N1 and C1−N2 bond lengths of the amidine >N2−C1(Ph)=N1− moiety demonstrates a strong localization of the >C1=N1− double bond. The N1−C1−N2 and C1−N1−P1 bond angles of 120.5(3)° and 119.2(2)°, respectively, are comparable to those found in the other two structurally characterized *N*-phosphino amidines $(Me_3Si)_2$N−C(Ph)=N−$PPh_2$[15] and *i*-$Pr_2$N−C(H)=N−$PPh_2$.[16]

The reaction of ruthenium(II) dimer [(*p*-cymene)$RuCl_2$]$_2$ with phosam **7a** afforded the complex [(*p*-cymene)$RuCl_2$($\eta^1$-**7a**)] (**8a**) in 75% yield (Scheme 2). In the $^1$H NMR spectrum, the singlet at 5.23 ppm integrating for four protons is characteristic of the *p*-cymene fragment coordinated to the ruthenium center.

The single-crystal crystallographic analysis confirmed the structure of the three-legged piano stool complex **8a** (Figure 5, Table 2). The coordination sphere of the ruthenium adopts a pseudo-octahedral geometry since the P1−Ru1−Cl1, P1−Ru1−Cl2, and Cl2−Ru1−Cl1 bond angles

(14) (a) Chivers, T.; McGregor; Parvez, M. *Inorg. Chem.* **1993**, *32*, 5119. (b) Wong, W.-K.; Sun, C.; Jiang, T.; Wong, W.-T.; Xue, F.; Mak, T. C. W. *J. Chem. Soc., Dalton Trans.* **1997**, 693. Note that only one X-ray crystallographic study in which the integrity of the structure of the starting N-phosphino amidine ligand was retained was described.

(15) A different procedure to prepare **1** was reported earlier by Manners et al. For convenient reasons we used *N*,*N*-diisopropylcyanamide as a starting reagent. Rivard, E.; Lough, A. J.; Chivers, T.; Manners, I. *Inorg. Chem.* **2004**, *43*, 802.

(16) Le, T. D.; Weyland, M.-C.; El-Harouch, Y.; Arquier, D.; Vendier, L.; Miqueu, K.; Sotiropoulos, J.-M.; Bastin, S.; Igau, A. *Eur. J. Inorg. Chem.* **2008**, 2577.

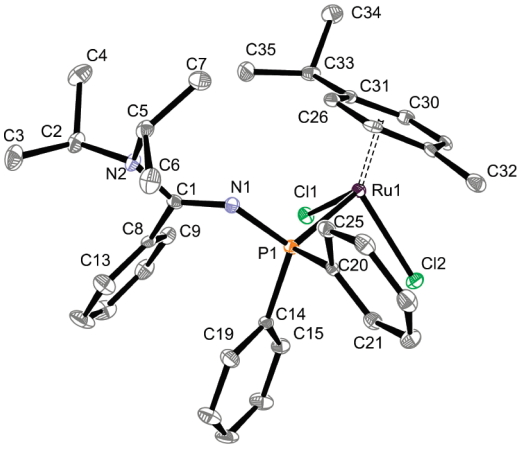


**Figure 5.** Molecular structure of $\eta^1$-*P N*-phosphino amidine ruthenium complex **8a**.

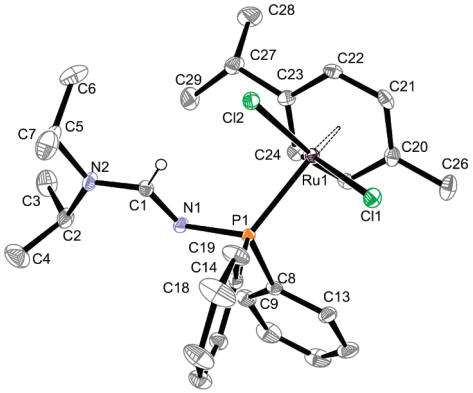


**Figure 6.** Molecular structure of $\eta^1$-*P N*-phosphino formamidine ruthenium complex **11**.

**Scheme 3**

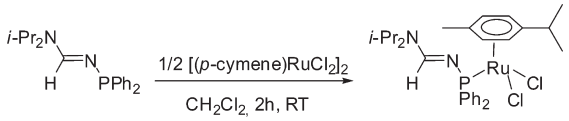


**10** **11**

are close to 90°, with the *p*-cymene ligand occupying three facial sites. As expected, the carbon atoms of the $\eta^6$-coordinated ring are coplanar. The Ru−P1 and the Ru−Cl distances in **8a** are in the range of the bond lengths reported for related [($\eta^6$-arene)Ru($PR_3$)$Cl_2$] complexes.[17] The Ru1−C30 and Ru1−C31 bond distances, respectively 2.239(5) and 2.230(4) Å, *trans* to the phosam ligand are elongated relative to those that are *trans* to the chlorine atoms, which is characteristic of the *trans*-bond-lengthening influence of a tertiary phosphine ligand.[17d] The C1−N1 and C1−N2 bond lengths and the N1−C1−N2 bond angle of the amidine fragment >N−C(Ph)=N− are comparable with those of the free ligand **7a**. Therefore, after complexation the ligand still showed a strong localization of the >C1=N1− double bond. The main characteristic structural feature of complex **8a** consists in the dramatic opening of the C1−N1−P1 bond angle up to 132.7(3)° and the significant shortening of the N1−P1 bond length compared to the free ligand **7a** (Table 2). As we mentioned above, the C1−N1 and C1−N2 bond lengths were not perturbed to any great extent upon coordination; therefore, the two main structural modifications could not be rationalized by the contribution of different mesomeric forms in the amidino fragment, which should induce significant modifications in both the C1−N1 and C1−N2 bond lengths. Considering the molecular drawing of **8a** (Figure 5) it is reasonable to propose a $\pi-\pi$ intramolecular arene interaction between the phenyl ring linked to the carbon atom of the amidine function and one of the two phenyl substituents on the phosphorus atom whose centroids are 3.70 Å apart from each other (interplane distance $d = 3.60$ Å, offset angle $\alpha = 14°$).[18] Therefore the coexistence of the effects of the $\eta^1$-*P* coordination mode on the ruthenium metal center and the $\pi-\pi$-arene interaction are responsible for the significant shortening of the N1−P1 bond length. The unusual large value of the C1−N1−P1 bond angle may be due to the steric hindrance in the second coordination sphere of the ruthenium(II) complex **8a**. In order to minimize these steric interactions, the amidine fragment *i*-$Pr_2$N−C(Ph)=N− is pushed away from the alkyl substituents linked to the *p*-cymene. This explanation is supported by the X-ray structure analysis recorded on the corresponding $\eta^1$-*P* formamidine ruthenium(II) complex **11** prepared in 87% isolated yield after reaction of phosfam ligand **10** with [(*p*-cymene)$RuCl_2$]$_2$ (Scheme 3, Figure 6, Table 2).

The structure of the $\eta^1$-*P* ruthenium(II) complexes **8a** and **11** have similar piano-stool geometry. Replacing the phenyl substituent on the methylene carbon atom by a hydrogen atom in the amidine moiety causes a decrease of the C1−N1−P1 bond angle value from 132.7(3)° in **8a** to 118.5(2)° in the $\eta^1$-*P* formamidine ruthenium(II) complex **11**, close to the value observed in the solid state of the free formamidine ligand **10** (115.7(2)°). Therefore, the comparison of the X-ray data of free **7a** and **10** and coordinated **8a** and **11** (form)amidine derivatives demonstrates that the *N*-phosphino amidine fragment is able to modify to a large extent its molecular structure to minimize the steric interactions.

Except in a few cases,[19] displacement of the arene ligand in ruthenium(II) half-sandwich complex **I** usually takes place above 120 °C. It is worthy to note that in our case the intramolecular arene substitution in complex **8a** occurred at a milder temperature of 80 °C in toluene for 20 h to afford the tethered $\eta^6$-arene-$\eta^1$-*P* phosphino amidine ruthenium(II) complex **9a** in 85% yield (Scheme 2). Complex **9a** precipitated during the reaction and was easily purified by filtration and isolated as a yellow-orange powder. As depicted in Scheme 2, it is also possible to synthesize **9a** in one step starting from a mixture of **7a** and [(*p*-cymene)$RuCl_2$]$_2$ heated at 80 °C overnight. The $^1$H NMR spectrum of the $\eta^6$-arene ring displayed three well-separated patterns, one doublet at

(17) (a) Caballero, A.; Jalón, F. A.; Manzano, B. R.; Espino, G.; Pérez-Manrique, M.; Mucientes, A.; Poblete, F. J.; Maestro, M. *Organometallics* **2004**, *23*, 5694. (b) Ghebreyessus, K. Y.; Nelson, J. H. *Organometallics* **2000**, *19*, 3387. (c) Faller, J. W.; Patel, B. P.; Albrizzio, M. A.; Curtis, M. *Organometallics* **1999**, *18*, 3096. (d) Bennett, M. A.; Robertson, G. B.; Smith, A. K. *J. Organomet. Chem.* **1972**, *43*, C41.

(18) Although experimentally well documented in the solid state, the characterization and quantification of the $\pi-\pi$ noncovalent interaction is still subject to discussion . Meyer, E. A.; Castellano, R. A.; Diederich, F. *Angew. Chem., Int. Ed.* **2003**, *42*, 1210, and references therein. Janiak, C. *J. Chem. Soc., Dalton Trans.* **2000**, 3885.

(19) To our knowledge, only very few arene substitution reactions occur at such a low temperature, <80 °C); see ref 8d and: (a) Faller, J. W.; D'Alliessi, D. G. *Organometallics* **2003**, *22*, 2749. (b) Cadierno, V.; Díez, J.; García-Álvarez, J.; Gimeno, J. *Chem. Commun.* **2004**, 1820. (c) Huber, D.; Kumar, P.G. A.; Pregosin, P. S.; Mikhel, I. S.; Mezzetti, A. *Helv. Chim. Acta* **2006**, *89*, 1696.

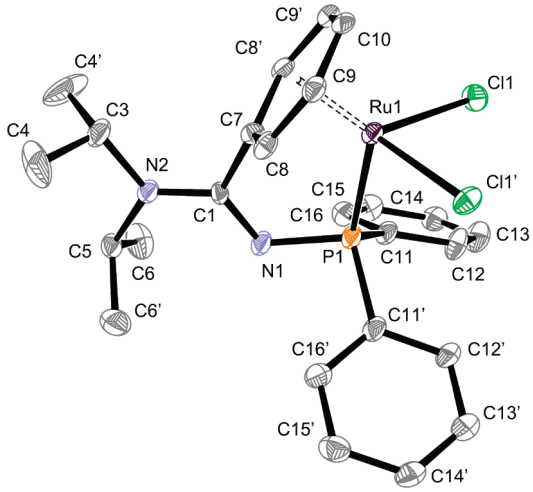


**Figure 7.** Molecular structure of $\eta^6$-arene-$\eta^1$-*P* *N*-phosphino amidine ruthenium complex **9a**.

5.26 ppm, a triplet at 5.94 ppm, and a multiplet centered at 6.32 ppm with integrated intensities of 2:2:1, respectively. A $^1$H−$^1$H COSY experiment allowed us to assign these resonances to the *ortho*, *meta*, and *para* protons, respectively. The upfield shielding of the arene ring protons in complex **9a** compared to **8a** is the signature of the $\eta^6$-coordination of the phenyl group to the ruthenium center. In the $^{13}$C NMR spectrum, four resonances were observed for the $\eta^6$-arene, one singlet and three doublets at 75.0 (s), 91.9 ($J_{CP}$ = 14.3 Hz), 95.7 ($J_{CP}$ = 3.8 Hz), and 122.2 ($J_{CP}$ = 6.4 Hz) ppm, respectively (Figure 7, Table 2).

As for complex **8a**, complex **9a** has a piano-stool geometry and the structure presents a mirror plane passing through atoms Ru1, C7, C10, C1, N1, and P1. The Ru1−Cl bond length of 2.3876(17) Å falls in the range of commonly observed for Ru1−Cl bond lengths for related complexes[10] and the Ru1−centroid distance is 1.684 Å. The Ru1−C10 bond length of 2.266(8) Å is significantly longer than the other Ru1−C bond lengths, which reflects the *trans* influence of the phosphine ligand. The arene carbon C7 connected to the imino carbon of the tether is displaced toward the ruthenium atom by 0.037 Å with respect to the plane defined by the carbons C8, C8′, C9, and C9′; the symmetrically opposite carbon C10 is displaced by 0.037 Å. The $\eta^6$-arene ring shows three sets of C−C bond lengths; the C7−C8 and C7−C8′ distances, 1.454(8) Å, are clearly longer than the other C−C distances, 1.420(10) and 1.393(9) Å. This bond lengthening can be attributed to the strain imposed by the tether. The projection of the ruthenium center onto the mean plane of the arene ring revealed a deviation of the latter of 0.11 Å from the centroid toward C7. This slight slippage is another proof of the strain generated by the tether. The C1−N1 bond length of the amidine fragment in **9a** is comparable with those of the linear complex **8a** and the free ligand **7a**. However, upon formation of the arene-tethered ruthenium(II) complex **9a**, we observed a significant shortening of the C1−N2 bond length and a contraction of the C1−N1−P1 bond angle to 115.6(7)°. The phosam ligand **7a** acts as an adaptive ligand that is able to modify to a large extent its molecular structure, which depends on whether the phosam ligand coordinates the metal in a $\eta^1$- or $\eta^6$:$\eta^1$-mode.

In order to further explore the coordination chemistry of the phosam class of ligands on ruthenium(II) metallic fragments,

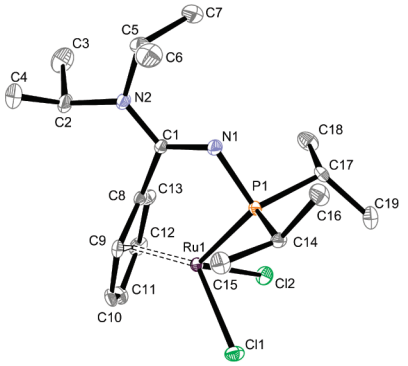


**Figure 8.** Molecular structure of $\eta^6$-arene-$\eta^1$-*P* *N*-phosphino amidine ruthenium complex **9b**.

and to study the structural parameters of the corresponding complexes, we have investigated the same sequence of reactions with phosam ligand **7b**. It was prepared in 85% isolated yield following the same procedure as described for **7a**.

The structure of phosam **7b** has a geometry very similar to **7a** (see Supporting Information, Table 2). The X-ray structure analysis revealed an *E*-stereoisomer. Compared to the other structurally characterized *N*-phosphino amidines, we observed in **7b** an even more pronounced difference of 0.070 Å between the C1−N1 and C1−N2 bond lengths of the amidine >N2−C1(Ph)=N1− moiety, demonstrating once again the strong localization of the >C1=N1− double bond. The corresponding [(*p*-cymene)$RuCl_2$ ($\eta^1$-**7b**)] (**8b**) complex was isolated in 70% yield upon addition of [(*p*-cymene)$RuCl_2]_2$ on **7b** (Scheme 2).

The single-crystal crystallographic analysis confirmed the structure of the three-legged piano stool complex **8b** with a pseudo-octahedral geometry around the ruthenium (see Supporting Information, Table 2). The Ru−P1 distance is slightly longer in **8b** compared to **8a**, and the large value of the C1−N1−P1 bond angle, up to 133.23(19)°, was again observed in **8b**. In the absence of the $\pi-\pi$ interaction observed in **8a**, the slight decrease of both C1−N1 and C1−N2 bond lengths was not observed in **8b**. All the other bond lengths and bond angles in **8b** are comparable to those found for **8a** (Table 2).

Displacement of the arene ligand in ruthenium(II) complex **8b** occurred at 80 °C to afford after 20 h the corresponding tethered $\eta^6$-arene-$\eta^1$-*P* phosphino amidine ruthenium(II) complex **9b** in 70% isolated yield (Scheme 2, Figure 8, Table 2).

The structure of phosam **9b** has a piano-stool geometry very similar to **9a**, and bond lengths and bond angles are highly comparable. The strain imposed by the tether was shown by a slight slippage of the arene ring. Another consequence generated by the tethered coordination mode concerns the amidine moiety. The C1−N1 bond length of the amidine fragment in **9b** is comparable with those of the linear complex **8b** and the free ligand **7b**. However, a significant shortening of the C1−N2 bond length in **9b** is observed as well as the contraction of the C1−N1−P1 bond angle to 116.4(3)°. Once again, the phosam derivative is able to modify to a large extent its molecular structure depending on whether it coordinates the metal in a $\eta^1$- or $\eta^6$:$\eta^1$-mode.

In order to have better insight into the geometrical and electronic structures of the free and coordinated methylenaminophosphine ligands R′C(Ph)=N−$PR_2$, DFT calculations at the B3LYP/SDD (Ru), 6-31G** (H, C, N, P, Cl)

**Table 3. Selected Bond Lengths (Å), Bond Angles (deg), Energetic Positions (eV) of the N1 and P1 Lone Pairs ($n_{N1}$ and $n_{P1}$), and $\pi_{C1=N1}$ and $\pi^*_{C1=N1}$ Molecular Orbitals[a] Calculated at the B3LYP/6-31G** Level of Theory for 1, 4, and 7a, and at B3LYP/Ru (SDD), 6-31G** (P, C, N, Cl, H) for 2, 5, and 8a, and 3, 6, and 9a**

| ligands | **1** | | | **4** | | | **7a** | | |
|---|---|---|---|---|---|---|---|---|---|
| $\eta^1$-*P* complexes | | **2** | | | **5** | | | **8a** | |
| $\eta^1,\eta^6$-complexes | | | **3** | | | **6** | | | **9a** |
| C1−N1 | 1.280 | 1.283 | 1.273 | 1.286 | 1.287 | 1.286 | 1.299 | 1.302 | 1.301 |
| P1−N1 | 1.766 | 1.725 | 1.780 | 1.733 | 1.702 | 1.756 | 1.736 | 1.701 | 1.722 |
| Ru−P1 | | 2.356 | 2.331 | | 2.383 | 2.330 | | 2.406 | 2.334 |
| C1−N1−P1 | 116.59 | 121.28 | 115.00 | 127.50 | 137.80 | 116.92 | 123.20 | 132.05 | 116.92 |
| N1−P1−Ru | | 109.66 | 98.55 | | 107.03 | 99.13 | | 113.97 | 105.20 |
| $\sum$P | 298.4 | 309.5 | | 303.8 | 312.3 | | 298.7 | 311.0 | |
| $n_{P1}$[a] | −5.71 | | | −5.51 | | | −5.18 | | |
| $\pi_{C1=N1}$[a] | −6.71 | −6.72 | −9.02 | −9.07 | −6.60 | −8.99 | −5.98 | −6.09 | −6.56 |
| $n_{N1}$[a] | −7.91 | −7.01 | −7.66 | −6.38 | −6.87 | −7.48 | −7.65 | −6.51 | −7.10 |
| $\pi^*_{C1=N1}$[a] | −1.53 | −1.86 | −1.87 | −1.42 | −1.91 | −2.27 | −0.62 | −0.54 | −0.85 |

[a] Main character in the MO.

level of theory were carried out on **1**−**6** and **7a**−**9a** derivatives; Table 3 summarizes the main calculated geometrical parameters and molecular orbitals (MO).

The global minimum on the potential energy surface (PES) for the *N*-phosphino aldimine ligand PhC(H)=N−$PPh_2$ (**1**) corresponds to an *E*-rotamer with the two lone pairs $n_{N1}$ and $n_{P1}$ in *trans* position. The phenyl ring and the C1N1P1 plane (2.8°) are coplanar, the C1−N1 bond length, 1.280 Å, corresponds to a double bond, and the bond angle at the nitrogen atom is found at 116.59°. When the hydrogen atom of the methylene PhC(H)= fragment in **1** is replaced by a second phenyl ring to form **4**, the phenyl ring opposite to the phosphorus atom remains nearly coplanar with the C1N1P1 plane (16.5°) and the other ring adopts a stacking-like position with one of the phenyl groups of the $-PPh_2$ moiety. In contrast to **1**, the lone pair of the phosphorus atom in **4** is located in the $\pi$ system plane (20° of deviation). Consequently, the geometry of the molecule is slightly modified. The bond angle at the nitrogen atom is increased and the N1−P1 bond length decreased because of a $\pi$ delocalization of the phosphorus lone pair, which cannot take place in **1**. The HOMO in **1** has mainly a phosphorus lone pair ($n_{P1}$) character in bonding combination with the imino nitrogen lone pair ($n_{N1}$) (Figure 9). For compound **4**, the main contribution to the HOMO remains the $n_{P1}$ but, in this case, in conjugation with the $\pi_{C1=N1}$ orbital (Figure 10). Considering the phosam ligand **7a**, the geometrical parameters found in the gas phase are consistent with those calculated for **1** and **4**. The global minimum on the PES is found to be the *E*-conformer with the phosphorus and imino nitrogen lone pairs in *trans* position. The amino nitrogen lone pair ($n_{N2}$) is not totally coplanar with the C1=N1 $\pi$ system (∼20°) but can, however, participate in the molecule stabilization by electronic delocalization. This is visualized in the plot of the MO (Figure 11) as well as in the NBO calculations ($n_{N2} \rightarrow \pi^*_{C1=N1}$ ∼47 kcal/mol; see Supporting Information). Indeed, the $\pi_{C1=N1}$ orbital is found to be in combination with the amino nitrogen lone pair (HOMO−1). The HOMO mainly corresponds to the bonding combination between $n_{N1}$ and $n_P$ lone pairs, with a weak contribution of the amino lone pair orbital ($n_{N2}$). In this case, the LUMO is less accessible than in **1** and **4** (−0.6 versus ∼−1.5 eV) because of the participation of the $n_{N2}$ in this interaction. The calculated bond lengths C1−N1 and C1−N2 are 1.299 and 1.384 Å, respectively.

Let us consider now the $\eta^1$-*P* methylenaminophosphine-type ligands ruthenium complexes **2**, **5**, and **8a**. The energetically most favorable structure for **2** is found to be the *E*-isomer with the Ru−P axis perpendicular to the N1−C1−$C_{ipso}$ plane. Compared with the free aldimine ligand **1**, the C1−N1 bond length remains at around 1.28 Å, and the phenyl ring is always coplanar with the N1−C1−P1 plane, in agreement with the NBO calculations, which show the stabilization interactions $\pi^{Ph}{}_{C=C} \rightarrow \pi^*_{C1=N1}/\pi_{C1=N1} \rightarrow \pi^{*Ph}{}_{C=C}$ are nearly equivalent (∼23 kcal·mol$^{-1}$) for **2** and **1** (see Supporting Information). The bond angle at the imino nitrogen atom is increased by 5°. Considering complex **5**, the calculated geometrical parameters (Table 3) are in accord with the solid state X-ray structural data (Table 1). The $\pi-\pi$ phenyl stacking interaction, which is also observed in the free ligand **4**, probably increased its stability. The value of the bond angle at the imino nitrogen increases from 127.5° in **4** to 137.8° in **5**. If we consider the amino-substituted ruthenium compound **8a**, among the two minima found on the PES, the more stable is the *E* isomer with the amino group coplanar to the $\pi$ system and the phenyl nearly perpendicular to the C1−N1−P1 plane in arene−arene $\pi$ interaction with one of the phenyl substituents connected to the phosphorus atom, in agreement with the X-ray structure. An opening of the bond angle around the imino nitrogen atom is observed with a large value of 132.05°.

As experimentally proposed, the shortening of the N1−P1 bond in complexes **2**, **5**, and **8a** compared respectively to **1**, **4**, and **7a** can be explained by two factors: the $\eta^1$-*P* ruthenium complexation of the phosphorus lone pair and the $\pi-\pi$ stacking. Indeed, if we consider compounds **1** and **2**, phosphorus complexation leads to a change in the hybridization of the phosphorus atom. The latter is less pyramidalized in the ruthenium complex than in the free ligand. Consequently, the s character of the P1−N1 bond in **2** (see Supporting Information) is increased (or p character decreased), leading to a shortening of the latter. Thus, the p character of the imino nitrogen lone pair is enhanced (see Supporting Information, NBO analyses), which involves an opening of the nitrogen bond angle around 5°. Replacing the hydrogen atom on the methylene fragment in **1** by a phenyl or the amino group *i*-$Pr_2N$ induces electronic and structural modifications of the corresponding methylenamino-type ligand. The favored calculated form of the $\eta^1$-*P* ruthenium complexes **5** and **8a** adopts a $\pi-\pi$ stacking arrangement

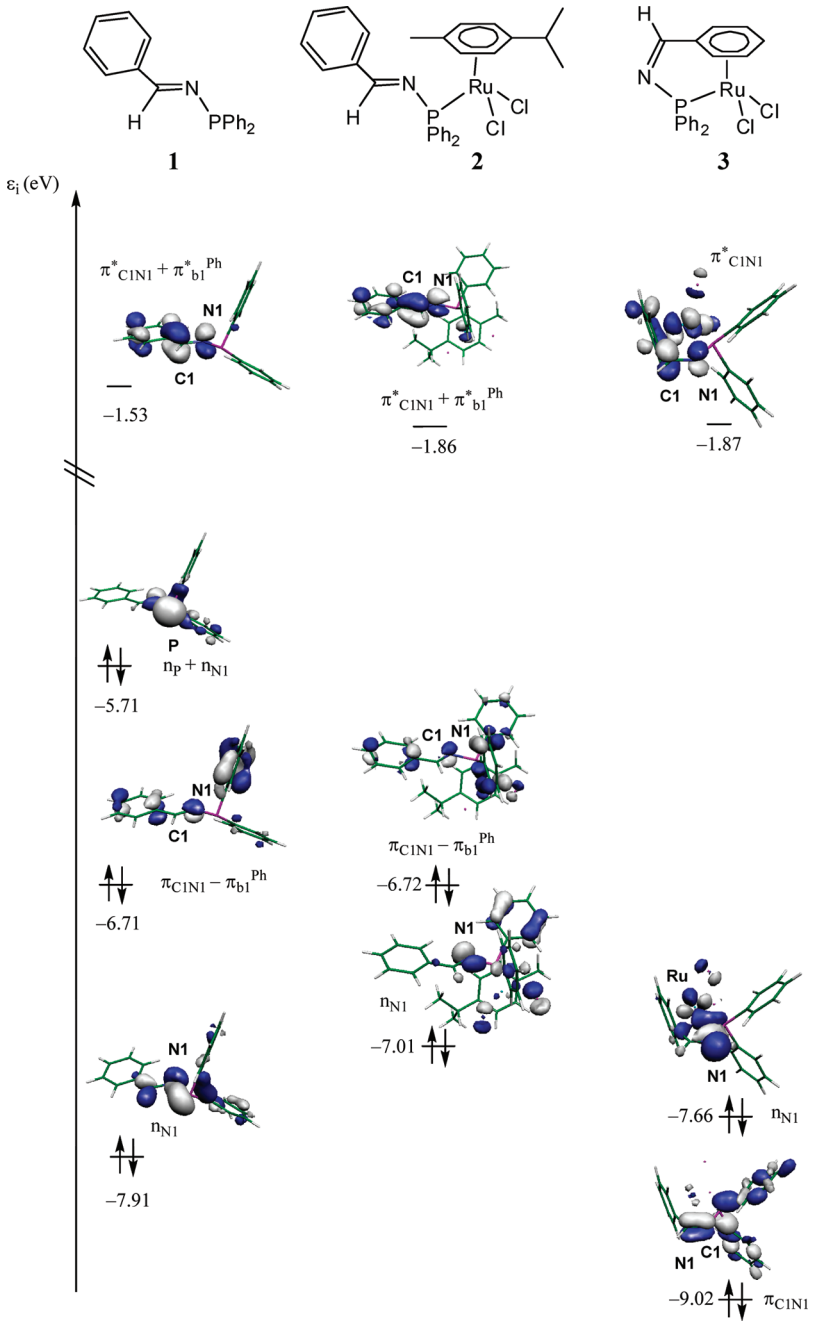


**Figure 9.** Plot (cutoff: 0.05), nature (main contribution), and energetic positions of the principal molecular orbitals (MO) at the B3LYP/SDD (Ru), 6-31G** (H, C, N, P, Cl) level of theory for compounds **1**, **2**, and **3**.

between the phenyl ring linked to the carbon atom of the methylene fragment and one of the two phenyl substituents on the phosphorus atom,[20] involving an electronic stabilization of the system. In addition to the $\eta^1$-*P* ruthenium complexation effect, this $\pi-\pi$ stacking enhances the widening of the imino nitrogen bond angle value by an additional 5°. It is noteworthy that the shortest N1−P1 distances are observed for **5** and **8a** (see Table 3).[21]

If we now consider the tethered $\eta^6$-arene-$\eta^1$-*P* ruthenium(II) complexes **3**, **6**, and **9a**, substitution of the hydrogen atom on the imino carbon in **3** by a phenyl or an amino group leads to a slight increase of the C=N bond length. This can be explained by the interaction between the $\pi$ system of the arene fragment or the lone pair of the amino group N*i*-$Pr_2$ and the $\pi_{C1=N1}$ system. This interaction already observed in the corresponding free ligands **4** and **7a** remains in the tethered complexes **6** and **9a**, respectively. The imino nitrogen bond angle C1−N1−P1 is more acute in **6** and **9a** compared to their corresponding free ligands and $\eta^1$-*P* ruthenium complexes because of the ring strain of the tethered structure. It is noteworthy that this bond angle is almost unchanged for the aldimine ligand **1** incorporated in tethered complex **3**.

(20) For compound **9a** another isomer without $\pi-\pi$ stacking exists on the potential energy surface. It is energetically less favorised ($\Delta G$: 9.1 kcal/mol between the two isomers), in agreement with the experimental data.

(21) The interaction between the p amino nitrogen lone pair $n_{N2}$ and the $\pi_{C1=N1}$ orbital in compound **8a** increases the C=N bond length; consequently the imino nitrogen bond angle C−N1−P is smaller than in compound **5**.

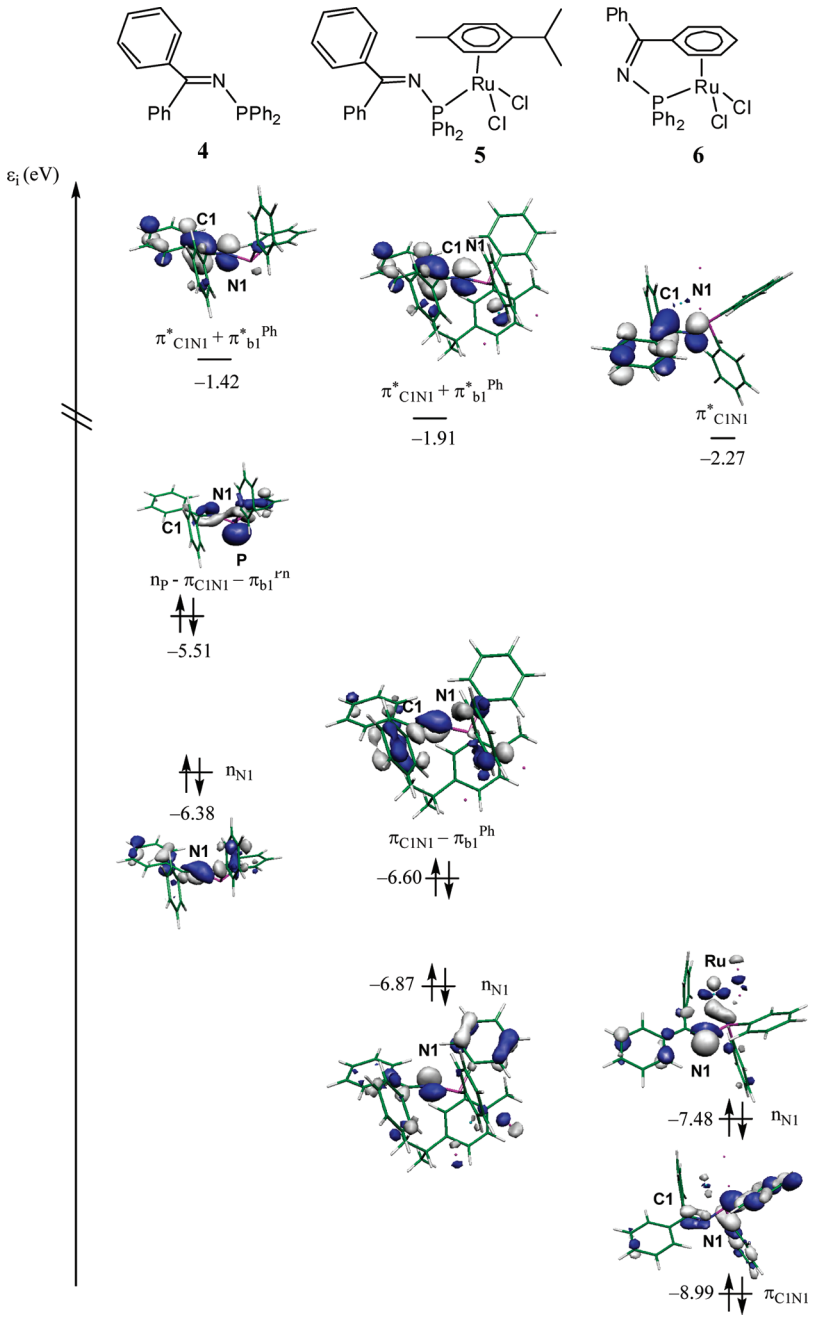


**Figure 10.** Plot (cutoff: 0.05), nature (main contribution), and energetic positions of the principal molecular orbitals (MO) at the B3LYP/SDD (Ru), 6-31G** (H, C, N, P, Cl) level of theory for compounds **4**, **5**, and **6**.

In order to have better insight into the electronic structure of the ruthenium complexes with the methylenaminophosphine-type ligands, we plotted the MO of compounds **2**, **3**, **5**, **6**, **8a**, and **9a** (Figures 9−11). Upon complexation on the ruthenium fragment [Ru(*p*-cymene)$Cl_2$], the energetic position of the $\pi_{C1=N1}$ orbital in the methylenaminophosphine-type ligands is not modified to any great extent except for the $\eta^1$-*P* ruthenium complex **5**, in which it is stabilized (for **4**, $\pi_{C1=N1}$ is in interaction with $n_P$). The calculated ionization energy of the imino nitrogen lone pair $n_{N1}$ in **2**, **5**, and **8a**, in the range 6.5−7.0 eV, is less accessible than for the $\pi_{C1=N1}$; however the energetic difference between these two MOs does not exceed 0.4 eV.

For the tethered complexes, the imino nitrogen lone pair $n_{N1}$ is in interaction with the $d_{xy}$(Ru) orbital (see Figures 9, 10, and 11). It is noteworthy that it is energetically less accessible than in the corresponding $\eta^1$-*P* ruthenium complexes (around 0.6 eV). The $\pi_{C1=N1}$ MO for tethered complexes **3** and **6** are a lot more stabilized (around 2.3 eV) than the ones for $\eta^1$-*P* complexes due to a decrease of $\pi_{C1=N1}/\pi^*_{C=C}{}^{ph}$ and/or $\pi_{C=C}{}^{ph}/\pi^*_{C1=N1}$ interactions, and consequently they become less accessible than the $n_{N1}$ lone pair MO. On the contrary, the interaction between the $\pi_{C1=N1}$ orbital and the amino lone pair $n_{N2}$ observed in **8a** remains when the tethered complex **9a** is formed. This observation explains why the energetic position of the $\pi_{C1=N1}$ orbital is only weakly affected (0.5 eV) in this case and why the order of the MO remains unchanged between the $\eta^1$-*P* untethered and the corresponding tethered complexes.

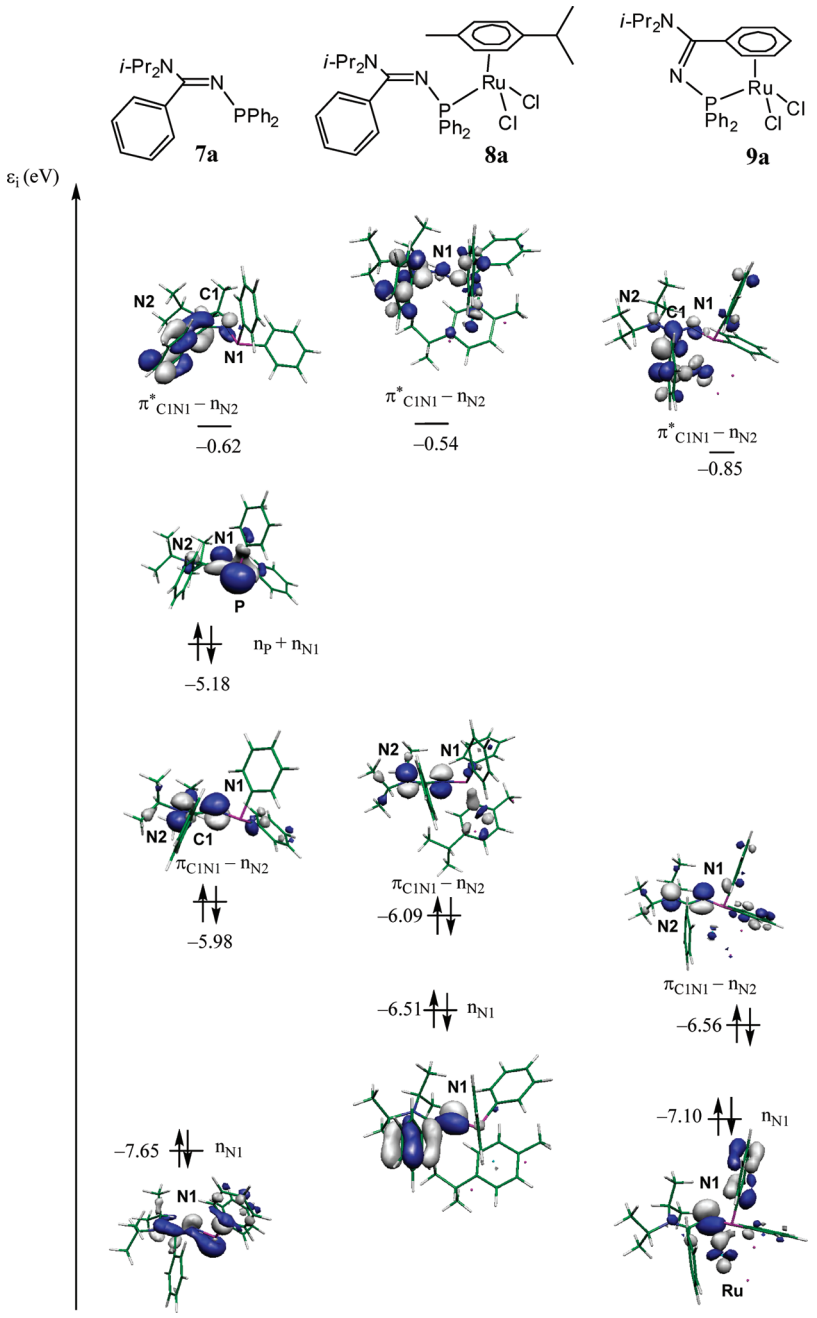


**Figure 11.** Plot (cutoff: 0.05), nature (main contribution), and energetic positions of the principal molecular orbitals (MO) at the B3LYP/SDD (Ru), 6-31G** (H, C, N, P, Cl) level of theory for compounds **7a**, **8a**, and **9a**.

In order to go further in the chemical behavior understanding of the $\eta^1$-*P* methylenaminophosphine-type ligands ruthenium complexes **2**, **5**, and **8a**, in the different attempts to get the corresponding tethered complexes **3**, **6**, and **9a**, we look at the energetic profile of the complexation reaction. Figure 12 summarizes the calculated energetic differences involved in the following sequence of reactions: [**1**, **4**, **7a**] + [(*p*-cymene)$RuCl_2$] → [**2**, **5**, **8a**] → [**3**, **6**, **9a**] + (*p*-cymene).

Formation reactions of $\eta^1$-*P* ruthenium complexes **2**, **5**, and **8a** incorporating methylenaminophosphine-type ligands **1**, **4**, and **7a** are exothermic (5 to 10 kcal/mol). However, when going from the $\eta^1$-*P* complexes to the corresponding tethered complexes, we note it is endothermic for complex **3**, incorporating the aldimine ligand **1**, and exothermic for the other two complexes **6** and **9a**. This result constitutes an argument to rationalize why the tethered complex **3** does not form starting from **2**. The energetic difference between the $\eta^1$-*P* ruthenium complexes **5** and **8a** and the tethered $\eta^6$-arene-$\eta^1$-*P* ruthenium complexes **6** and **9a**, respectively, is more pronounced for **8a**/**9a** than **5**/**6** (15 versus 9 kcal·mol$^{-1}$), which is consistent with the experimental results. Moreover, to form the tethered complex starting from **2**, it is necessary to rotate the phenyl ring of the methylene fragment $Ph_2C$= in a near perpendicular orientation to the $\pi_{C1=N1}$ orbital system. Consequently, the stabilizing $\pi_{C1=N1} \rightarrow \pi^{*Ph}{}_{C=C}$ and $\pi^{Ph}{}_{C=C} \rightarrow \pi^{*}{}_{C1=N1}$ interactions are lost during the last step of the coordination process (see Supporting Information: $\sum\pi$ stabilizing interactions = 27−28 kcal/mol in **1** and **2** and 0 kcal/mol in **3**). In

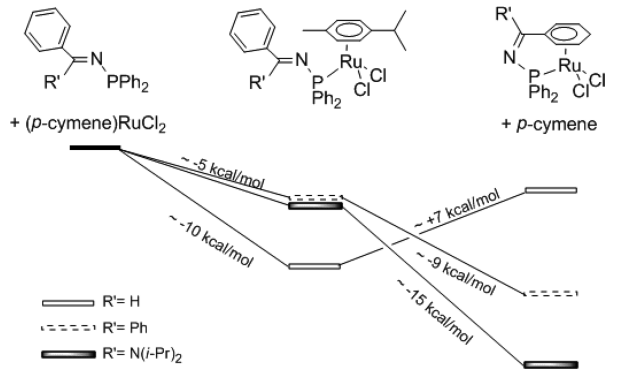


**Figure 12.** Free Gibbs energetic differences ($\Delta G$ in kcal/mol) involved in the formation of tethered $\eta^6$-arene-$\eta^1$-*P* ruthenium-(II) complexes incorporating methylenaminophosphine-type ligands.

the same way, these two previous interactions are involved in the stabilization effects of the $\eta^1$-*P* ruthenium complex **5**, whereas in the corresponding tethered complex **6**, solely the $\pi_{C1=N1} \rightarrow \pi^{*Ph}_{C=C}$ interaction is present, allowing only a weak stabilization of the $\pi$ system. Indeed, NBO analyses (see Supporting Information) show the stabilizing interactions involving the $\pi$ system go from around 23 kcal/mol in **4** and **5** to 7 kcal/mol in **6**. Finally, in **9a**, the amino group is nearly coplanar to the $\pi$ system with a C1N2/C1N1 dihedral angle of 3° compared to 14° in **8a**. Consequently, the $n_{N2} \rightarrow \pi^*_{C1=N1}$ interaction remains present in the *N*-phosphino amidino complexes, allowing a $\pi$ system stabilization, which is even more efficient in the tethered complex because of a better overlap. NBO analyses (see Supporting Information: $n_{N2} \rightarrow \pi^*_{C1=N1} \approx 60$ kcal/mol in **8a** and 72 kcal/mol in **9a**) as well as the plot of the LUMO (Figure 11) confirm the presence of a strong stabilizing interaction allowing a system stabilization in **9a**. In summary, the highest energetic difference between the $\eta^1$-*P* and the tethered $\eta^6$-arene-$\eta^1$-*P* coordination mode observed for the phosam ligand is a reasonable explanation for the straightforward preparation of the tetehered complexes **9a**,**b** compared to **3** and **6**. Moreover conservation of the $\pi$ system stabilization in tethered complexes incorporating phosam ligands is also in favor of the formation of **9a**,**b**.

## Conclusions

In conclusion, we have prepared and structurally characterized $\eta^1$-*P* ruthenium(II) complexes **2**, **5**, **7a**, and **7b** incorporating methylenaminophosphine-type ligands R′C(Ph)=N−$PR_2$ (R = Ph, R′ = H (**1**), R = Ph, R′ = Ph (**4**), R = Ph, R′ = *i*-$Pr_2N$ (**7a**), R = *i*-Pr, R′ = *i*-$Pr_2N$ (**7b**)). Our experimental results and theoretical calculations showed that complexes **2** and **5** are not good precursors to form their corresponding tethered $\eta^6$-arene-$\eta^1$-*P* ruthenium(II) complexes **3** and **6**. However, we developed a straightforward synthesis of new tethered ruthenium(II) complexes **9a** and **9b** incorporating *N*-phosphino amidines (phosam) **7a** and **7b** as chelating ligands. Interestingly, the displacement of the $\eta^6$-*p*-cymene ligand by the phenyl substituent of the *N*-phosphino amidine occurs under relatively mild conditions compared to what is usually observed for *p*-cymene substitution reaction. We have observed by X-ray crystallographic analyses that the *N*-phosphino amidine ligands **7a** and **7b** act as adaptive ligands that are able to modulate to a large extent their C1−N1, C1−N2, and N1−P1 bond distances and C1−N1−P1 bond angle depending on the coordination mode, untethered $\eta^1$-*P* in **8a** and **8b** or tethered $\eta^6$-arene-$\eta^1$-*P* in **9a** and **9b**. The imino nitrogen atom =N1− of the amidine function behaves as a universal joint, which optimizes the ability of the phosphorus atom to bind the metal. Theoretical studies showed that the interaction between the $\pi_{C1=N1}$ and the amino lone pair $n_{N2}$ orbitals remains when the tethered complex **9a** is formed from the corresponding $\eta^1$-*P* **8a** complex, allowing a $\pi$ system stabilization, which can be one of the reasons that isolation of this compound is straightforward. NBO analyses as well as the plot of the LUMO confirm these results. Moreover, the calculated energetic differences involved in the sequence of reactions [**1**, **4**, **7a**] + [(*p*-cymene)$RuCl_2$] → [**2**, **5**, **8a**] → [**3**, **6**, **9a**] + (*p*-cymene) clearly demonstrated the pronounced preference for the formation of the tethered complex **9a** (last step: exothermic reaction). Our studies showed that the presence of the amino group linked to the imino carbon atom in methylenaminophosphine-type ligands is crucial for the preparation of the tethered $\eta^6$-arene-$\eta^1$-*P* ruthenium(II) complexes. Therefore, the *N*-phosphino amidine skeleton is particularly appropriate as a building block for the extension to chiral tethered complexes. Preparation of cationic chiral tethered $\eta^6$-arene-$\eta^1$-*P* ruthenium(II) complexes and their evaluation in asymmetric catalysis are under active investigations in our group.

## Experimental Section

**General Information.** All reactions were conducted under an inert atmosphere of dry argon using standard Schlenk-line techniques. Solvents were dried, distilled, and degassed following conventional methods prior to use; $Ph_2PCl$ was distilled prior to use. All other commercial chemicals were used as received. Methylenaminophosphines $PhC(H)NPPh_2$[12] and $Ph_2CNPPh_2$[13] were synthesized as previously described.

NMR spectra were recorded on a Bruker AV 300 and on a Bruker AC 200 spectrometer. Chemical shifts for $^1H$ and $^{13}C$ are referenced to residual solvent resonances used as an internal standard and reported relative to $SiMe_4$. $^{31}P$ chemical shifts are reported relative to external aqueous 85% $H_3PO_4$. All the $^1H$ and $^{13}C$ signals were assigned on the basis of chemical shifts, spin−spin coupling constants, splitting patterns, and signal intensities and by using 2D experiments as $^1H-^1H$ COSY45 and $^1H-^{13}C$ HMQC experiments. All spectra were recorded at ambient probe temperature. Infrared spectra were recorded by using KBr pellets on a Perkin-Elmer GX 2000 spectrometer. Mass spectra were recorded on a TSQ7000 instrument from ThermoElectron. Melting points were obtained using an Electrothermal digital melting point apparatus and are uncorrected.

**Structure Determination and Refinement for Compounds 2, 5, 7−9, and 11.** Data were collected at low temperature (180 K) on an Xcalibur Oxford Diffraction diffractometer using graphite-monochromated Mo Kα radiation ($\lambda$ = 0.71073 Å) and equipped with an Oxford Instrument cooler device for compound **7a** (CCDC 689855), complex **8a** (CCDC 689856), compound **7b** (CCDC 717809), and complex **9b** (CCDC 717810), on an IPDS Stoe diffractometer using graphite-monochromated Mo Kα radiation ($\lambda$ = 0.71073 Å) and equipped with an Oxford Cryosystems cryostream cooler device for complexes **9a** (CCDC 689857), **8b** (CCDC 717810), and **11** (CCDC 717812) and on a Kappa APEX II Bruker diffractometer using graphite-monochromated Mo Kα radiation ($\lambda$ = 0.71073 Å) and equipped with an Oxford Cryosystems cryostream cooler device for complexes **2** (CCDC 717807) and **5** (CCDC 717808). The final unit cell parameters have been obtained by means of a least-squares

refinement. The structures have been solved by direct methods using SIR92[22] and refined by means of least-squares procedures on $F^2$ with the aid of the program SHELXL97[23] included in the softwares package WinGX version 1.63.[24] The atomic scattering factors were taken from International Tables for X-ray Crystallography.[25] All hydrogens atoms were geometrically placed and refined by using a riding model.

All non-hydrogens atoms were anisotropically refined, and in the last cycles of refinement a weighting scheme was used, where weights are calculated from the following formula: $w = 1/[\sigma^2(F_o^2) + (aP)^2 + bP]$ where $P = (F_o^2 + 2F_c^2)/3$.

Drawing of molecules were performed with the program ORTEP32[26] with 30% probability displacement ellipsoids for non-hydrogen atoms. Hydrogen atoms have been omitted for clarity.

**Synthesis of Complex 2.** A solution of $[(p\text{-cymene})RuCl_2]_2$ (84 mg, 0.14 mmol) in 7 mL of dichloromethane was slowly added to a solution of HC(Ph)=N−$PPh_2$ (**1**) (94 mg, 0.32 mmol) in 3 mL of dichloromethane at room temperature. The reaction mixture was allowed to stir for 3 h, the solvent was removed, and the orange solid was washed with pentane (3 × 10 mL) and dried under vacuum to give 90% (150 mg) yield of **2**. Suitable crystals were obtained from a saturated dichloromethane solution at 4 °C. Mp: 181−183 °C (dec). $^1$H NMR (300.1 MHz, $CD_2Cl_2$): $\delta$ 8.34 (d, $J_{H-P}$ = 29.7 Hz, 1H, C(*H*)=N−P), 8.00−7.91 (m, 5H, $C_6H_5$), 7.58−7.41 (m, 10H, $C_6H_5$), 5.28 (d, $J_{H-H}$ = 6.1 Hz, 2H, $C_6H_{4(p\text{-cymene})}$), 5.22 (d, $J_{H-H}$ = 6.1 Hz, 2H, $C_6H_{4(p\text{-cymene})}$), 2.72 (sept, $J_{H-H}$ = 6.9 Hz, 1H, C*H*$(CH_3)_{2(p\text{-cymene})}$), 1.80 (s, 3H, C*H*$_{3(p\text{-cymene})}$), 1.03 (d, $J_{H-H}$ = 6.9 Hz, 6H, CH(C*H*$_3)_{2(p\text{-cymene})}$) ppm. $^{13}$C{$^1$H} NMR (75.5 MHz, $CD_2Cl_2$): $\delta$ 170.1 (d, $J_{C-P}$ = 8.2 Hz, *C*(Ph)=N), 136.5 (d, $J_{C-P}$ = 21.9 Hz, $C_6H_5$), 135.0 (d, $J_{C-P}$ = 48.7 Hz, $C_6H_5$), 133.6 (d, $J_{C-P}$ = 9.7 Hz, $C_6H_5$), 132.7 (s, $C_6H_5$), 130.6 (d, $J_{C-P}$ = 2.4 Hz, $C_6H_5$), 129.4 (s, $C_6H_5$), 128.8 (s, $C_6H_5$), 127.8 (d, $J_{C-P}$ = 9.9 Hz, $C_6H_5$), 109.4 (s, $C_6H_{4(p\text{-cymene})}$), 95.8 (s, $C_6H_{4(p\text{-cymene})}$), 91.2 (d, $J_{C-P}$ = 4.4 Hz, $C_6H_{4(p\text{-cymene})}$), 85.8 (d, $J_{C-P}$ = 5.9 Hz, $C_6H_{4(p\text{-cymene})}$), 30.3 (s, *C*H$(CH_3)_{2(p\text{-cymene})}$), 21.5 (s, CH(*C*H$_3)_{2(p\text{-cymene})}$), 17.1 (s, *C*H$_{3(p\text{-cymene})}$) ppm. $^{31}$P{$^1$H} NMR (121.5 MHz, $CD_2Cl_2$): $\delta$ 59.9 ppm. DCI MS ($CH_4$, positive mode): *m*/*z* 595 $[M]^+$, 560 $[M - Cl]^+$. Crystal data: see Supporting Information.

**Synthesis of Complex 5.** A solution of $[(p\text{-cymene})RuCl_2]_2$ (75 mg, 0.12 mmol) in 7 mL of dichloromethane was slowly added to a solution of $Ph_2C$=N−$PPh_2$ (**4**) (100 mg, 0.27 mmol) in 3 mL of dichloromethane at room temperature. The reaction mixture was allowed to stir for 3 h, the solvent was removed, and the orange solid was washed with pentane (3 × 10 mL) and dried under vacuum to give 95% (153 mg) yield of **5**. Suitable crystals were obtained by a slow diffusion of pentane into a solution of the complex in dichloromethane at room temperature. $^1$H NMR (300.1 MHz, $CD_2Cl_2$): $\delta$ 7.94−7.12 (m, 20H, $C_6H_5$), 5.41−5.34 (m, 4H, $C_6H_4$), 2.75 (sept, 1H, $J_{H-H}$ = 6.9 Hz, C*H*$(CH_3)_{2(p\text{-cymene})}$), 1.71 (s, 3H, C*H*$_{3(p\text{-cymene})}$), 0.92 (d, 6H, $J_{H-H}$ = 6.9 Hz, CH(C*H*$_3)_{2(p\text{-cymene})}$) ppm. $^{13}$C{$^1$H} NMR (75.5 MHz, $CD_2Cl_2$): $\delta$ 174.6 (d, $J_{C-P}$ = 14.3 Hz, *C*$(Ph)_2$=N), 137.7 (d, $J_{C-P}$ = 13.4 Hz, $C_6H_5$), 136.5 (d, $J_{C-P}$ = 47.5 Hz, $C_6H_5$), 133.1 (d, $J_{C-P}$ = 10.0 Hz, $C_6H_5$), 132.3 (d, $J_{C-P}$ = 10.8 Hz, $C_6H_5$), 131.7 (d, $J_{C-P}$ = 10.9 Hz, $C_6H_5$), 130.2 (s, $C_6H_5$), 129.7 (d, $J_{C-P}$ = 2.5 Hz, $C_6H_5$), 129.3 (s, $C_6H_5$), 127.7 (s, $C_6H_5$), 127.2 (d, $J_{C-P}$ = 10.1 Hz, $C_6H_5$), 108.3 (s, $C_6H_{4(p\text{-cymene})}$), 95.0 (s, $C_6H_{4(p\text{-cymene})}$), 92.1 (d, $J_{C-P}$ = 4.7 Hz, $C_6H_{4(p\text{-cymene})}$), 85.9 (d, $J_{C-P}$ = 6.0 Hz, $C_6H_{4(p\text{-cymene})}$), 30.1 (s, *C*H$(CH_3)_{2(p\text{-cymene})}$), 21.2 (s, CH(*C*H$_3)_{2(p\text{-cymene})}$), 17.1 (s, *C*H$_{3(p\text{-cymene})}$) ppm. $^{31}$P{$^1$H} NMR (121.5 MHz, $CD_2Cl_2$): $\delta$ 44.1 ppm. DCI MS ($CH_4$, positive mode): *m*/*z* 671 $[M]^+$, 636 $[M - Cl]^+$. Crystal data: see Supporting Information.

**General Procedure for the Synthesis of Ligands 7a,b.** A solution of *N*,*N*-diisopropylcyanamide (1.80 mL, 11.9 mmol) in 10 mL of diethyl ether was added slowly to a solution of phenyllithium (5.95 mL, 2.0 M solution in $Bu_2O$, 11.9 mmol) in 20 mL of diethyl ether at −40 °C. The reaction mixture was stirred for 1 h at −40 °C to give a yellow solution. The chlorophosphane ($Ph_2PCl$, 2.15 mL, 11.9 mmol or *i*-$Pr_2PCl$, 1.89 mL, 11.9 mmol) was then added dropwise, and the reaction mixture was allowed to warm to room temperature. A white precipitate of LiCl was formed during the reaction. The solvent was removed and pentane was added. The reaction mixture was stirred for 10 min. The precipitate was allowed to settle and the mother liquor was decanted. This procedure was repeated three times. The pentane fractions were combined and the solvent was removed to give respectively 82% (3.79 g) and 85% (3.24 g) yields of **7a** and **7b**. Suitable crystals of **7a** and **7b** were obtained from a saturated pentane solution at room temperature and at −10 °C, respectively.

**7a.** $^{15}$ $^{31}$P{$^1$H} NMR (121.5 MHz, $C_6D_6$): $\delta$ 47.1 ppm. Crystal data: see Supporting Information.

**7b.** $^1$H NMR (300.1 MHz, $C_6D_6$): $\delta$ 7.29−7.24 (m, 3H, $C_6H_5$), 7.16−7.11 (m, 2H, $C_6H_5$), 3.70−3.40 (br m, 2H, NC*H*$(CH_3)_2$), 1.89 (sept d, 2H, $J_{H-H}$ = 7.0 Hz and $J_{H-P}$ = 1.6 Hz, PC*H*$(CH_3)_2$), 1.85−1.50 (br m, 6H, NCH(C*H*$_3)_2$), 1.35 (dd, $J_{H-H}$ = 6.9 Hz and $J_{H-P}$ = 9.8 Hz, 6H, PCH(C*H*$_3)_2$), 1.19 (dd, $^3J_{H-H}$ = 7.1 Hz and $^3J_{H-P}$ = 14.3 Hz, 6H, PCH(C*H*$_3)_2$), 1.10−0.70 (br m, 6H, NCH(C*H*$_3)_2$) ppm. $^{13}$C{$^1$H} NMR (62.9 MHz, $C_6D_6$): $\delta$ 167.7 (d, $J_{C-P}$ = 29.6 Hz, *C*(Ph)=N), 139.7 (d, $J_{C-P}$ = 7.9 Hz, $C_6H_5$), 128.8 (s, $C_6H_5$), 128.0 (s, $C_6H_5$), 127.8 (s, $C_6H_5$), 50.9 (br s, N*C*H$(CH_3)_2$), 46.9 (br s, N*C*H$(CH_3)_2$), 28.1 (d, $J_{C-P}$ = 13.8 Hz, P*C*H$(CH_3)_2$), 21.4 (s, NCH(*C*H$_3)_2$), 19.7 (d, $J_{C-P}$ = 19.7 Hz, PCH(*C*H$_3)_2$), 19.0 (d, $J_{C-P}$ = 8.0 Hz, PCH(*C*H$_3)_2$) ppm. $^{31}$P{$^1$H} NMR (121.5 MHz, $C_6D_6$): $\delta$ 69.1 ppm. DCI MS ($NH_3$/positive mode): *m*/*z* 321 $[M + H]^+$. Crystal data: see Supporting Information.

**General Procedure for the Synthesis of Complexes 8a,b.** A solution of $[(p\text{-cymene})RuCl_2]_2$ (85 mg, 0.139 mmol) in 7 mL of dichloromethane was slowly added to a solution of *i*-$Pr_2$N−C(Ph)=N−$PPh_2$ (**7a**) (108 mg, 0.278 mmol) or *i*-$Pr_2$N−C(Ph)=N−P*i*-$Pr_2$ (**7b**) (89 mg, 0.278 mmol) in 3 mL of dichloromethane at room temperature. The reaction mixture was allowed to stir for 3 h, the solvent was removed, and the orange solid was washed with diethyl ether (3 × 10 mL) and dried under vacuum to give respectively 75% (144 mg) and 70% (122 mg) yields of **8a** and **8b**. Suitable crystals were obtained from a saturated dichloromethane solution of **2a** and **2b** at room temperature.

**8a.** Mp: 221−226 °C (dec). $^1$H NMR (300.1 MHz, $CDCl_3$): $\delta$ 7.69−7.62 (m, 4H, $C_6H_5$), 7.18−7.06 (m, 6H, $C_6H_5$), 6.95−6.83 (m, 5H, $C_6H_5$), 5.23 (br s, 4H, $C_6H_{4(p\text{-cymene})}$), 4.00 (br m, 1H, NC*H*$(CH_3)_2$), 3.46 (br m, 1H, NC*H*$(CH_3)_2$), 2.87 (sept, $J_{H-H}$ = 6.9 Hz, 1H, C*H*$(CH_3)_{2(p\text{-cymene})}$), 1.85 (br m, 6H, NCH(C*H*$_3)_2$), 1.68 (s, 3H, C*H*$_{3(p\text{-cymene})}$), 1.09 (d, $J_{H-H}$ = 6.9 Hz, 6H, CH(C*H*$_3)_{2(p\text{-cymene})}$), 1.02 (d, $J_{H-H}$ = 6.8 Hz, 6H, NCH(C*H*$_3)_2$) ppm. $^{13}$C{$^1$H} NMR (75.5 MHz, $CDCl_3$): $\delta$ 164.1 (s, *C*(Ph)=N), 140.2 (d, $J_{C-P}$ = 47.3 Hz, $C_6H_5$), 135.2 (br s, $C_6H_5$), 133.2 (d, $J_{C-P}$ = 9.8 Hz, $C_6H_5$), 128.7 (d, $J_{C-P}$ = 2.3 Hz, $C_6H_5$), 127.7 (s, $C_6H_5$), 126.7 (d, $J_{C-P}$ = 9.7 Hz, $C_6H_5$), 107.5 (s, $C_6H_{4(p\text{-cymene})}$), 92.8 (s, $C_6H_{4(p\text{-cymene})}$), 92.2 (d, $J_{C-P}$ = 4.8 Hz, $C_6H_{4(p\text{-cymene})}$), 85.6 (d, $J_{C-P}$ = 6.5 Hz, $C_6H_{4(p\text{-cymene})}$), 51.1 (br s, N*C*H$(CH_3)_2$), 46.7 (s, N*C*H$(CH_3)_2$), 29.6 (s, *C*H$(CH_3)_{2(p\text{-cymene})}$), 21.8 (s, CH(*C*H$_3)_{2(p\text{-cymene})}$), 20.9 (s, NCH(*C*H$_3)_2$), 17.1 (s, *C*H$_{3(p\text{-cymene})}$) ppm. $^{31}$P{$^1$H} NMR (121.5 MHz, $CDCl_3$): $\delta$ 44.9 (br s) ppm. DCI MS ($CH_4$, positive mode): *m*/*z* 560 $[M - p\text{-cymene}]^+$,

(22) *SIR92*, A program for crystal structure solution. Altomare, A.; Cascarano, G.; Giacovazzo, C.; Guagliardi, A. *J. Appl. Crystallogr.* **1993**, *26*, 343.

(23) Sheldrick, G. M. *SHELX97* [includes SHELXS97, SHELXL97, CIFTAB], Programs for Crystal Structure Analysis (Release 97-2) ; Institüt für Anorganische Chemie der Universität: Göttingen, Germany, 1998.

(24) *WINGX*-1.63 Integrated System of Windows Programs for the Solution, Refinement and Analysis of Single Crystal X-Ray Diffraction Data. Farrugia, L. J. *J. Appl. Crystallogr.* **1999**, *32*, 837.

(25) *International Tables for X-Ray Crystallography*; Kynoch Press: Birmingham, England, 1974; Vol. *IV*.

(26) *ORTEP3* for Windows. Farrugia, L. J. *J. Appl. Crystallogr.* **1997**, *30*, 565.

525 $[M - Cl - p\text{-cymene}]^+$. IR (KBr): $\nu$ 3055 (m), 3043 (m), 2960 (m), 1603 (w), 1573 (s), 1550 (s), 1433 (s), 1371 (s), 1335 (s), 1093 (m), 791 (s), 698 (s), 527 (s) $cm^{-1}$. Crystal data: see Supporting Information.

**8b.** Mp: 264−265 °C (dec). $^1H$ NMR (200.1 MHz, $CDCl_3$): $\delta$ 7.54−7.25 (m, 5H, $C_6H_5$), 5.55−5.47 (m, 4H, $C_6H_{4(p\text{-cymene})}$), 4.22−4.00 (br m, 1H, $NCH(CH_3)_2$), 3.90−3.56 (br m, 1H, $NCH(CH_3)_2$), 2.91 (sept, $J_{H-H}$ = 7.0 Hz, 1H, $CH(CH_3)_{2(p\text{-cymene})}$), 2.35−2.14 (m, 2H, $PCH(CH_3)_2$), 2.14 (s, 3H, $CH_{3(p\text{-cymene})}$), 1.74−1.53 (br m, 6H, $NCH(CH_3)_2$), 1.31 (d, $J_{H-H}$ = 7.0 Hz, 6H, $CH(CH_3)_{2(p\text{-cymene})}$), 1.27−1.10 (m, 6H, $NCH(CH_3)_2$), 1.05 (dd, $J_{H-H}$ = 7.0 Hz and $J_{H-P}$ = 14.4 Hz, 6H, $PCH(CH_3)_2$), 0.92 (dd, $J_{H-H}$ = 7.1 Hz and $J_{H-P}$ = 13.8 Hz, 6H, $PCH(CH_3)_2$) ppm. $^{13}C\{^1H\}$ NMR (50.3 MHz, $CDCl_3$): $\delta$ 161.7 (d, $J_{C-P}$ = 5.8 Hz, C(Ph)=N), 137.5 (d, $J_{C-P}$ = 3.72 Hz, $C_6H_5$), 129.4 (s, $C_6H_5$), 129.0 (s, $C_6H_5$), 128.1 (s, $C_6H_5$), 109.0 (s, $C_6H_{4(p\text{-cymene})}$), 95.7 (s, $C_6H_{4(p\text{-cymene})}$), 87.5 (d, $J_{C-P}$ = 3.5 Hz, $C_6H_{4(p\text{-cymene})}$), 85.2 (d, $J_{C-P}$ = 4.3 Hz, $C_6H_{4(p\text{-cymene})}$), 52.6 (s, $NCH(CH_3)_2$), 46.6 (s, $NCH(CH_3)_2$), 30.3 (s, $CH(CH_3)_{2(p\text{-cymene})}$), 28.0 (d, $J_{C-P}$ = 24.7 Hz, $PCH(CH_3)_2$), 22.6 (s, $CH(CH_3)_{2(p\text{-cymene})}$), 21.6 (s, $NCH(CH_3)_2$), 19.6 (d, $J_{C-P}$ = 35.2 Hz, $PCH(CH_3)_2$), 17.9 (s, $CH_{3(p\text{-cymene})}$) ppm. $^{31}P\{^1H\}$ NMR (81.0 MHz, $CDCl_3$): $\delta$ 74.5 ppm. DCI MS ($CH_4$, positive mode): $m/z$ 492 $[M - p\text{-cymene}]^+$, 457 $[M - Cl - p\text{-cymene}]^+$. IR (KBr): $\nu$ 2996 (w), 2964 (m), 2924 (m), 2869 (w), 1579 (m), 1558 (s), 1367 (m), 1321 (m), 1034 (m) $cm^{-1}$. Crystal data: see Supporting Information.

**General Procedure for the Synthesis of Complexes 9a,b.** A solution of complex **8a** (99 mg, 0.14 mmol) or **8b** (58 mg, 0.09 mmol) in 5 mL of toluene was stirred at 80 °C for 20 h. An orange precipitate was formed, the reaction mixture was allowed to cool to room temperature, and the red surpernatant solution was filtered off. The orange solid was dried under vacuum to give respectively 85% (67 mg) and 70% (32 mg) yields of **9a** and **9b**. Suitable crystals of **9a** and **9b** were obtained from saturated dichloromethane solutions at −18 °C. **9a** was also obtained by stirring a solution of $[(p\text{-cymene})RuCl_2]_2$ (85 mg, 0.139 mmol) and $i\text{-}Pr_2N{-}C(Ph){=}N{-}PPh_2$ (**7a**) (108 mg, 0.278 mmol) in 5 mL of toluene at 80 °C for 20 h. **9a** was isolated in 72% yield.

**9a.** Mp: 245−247 °C (dec). $^1H$ NMR (300.1 MHz, $CD_2Cl_2$): $\delta$ 7.79−7.72 (m, 4H, $C_6H_5$), 7.42−7.39 (m, 6H, $C_6H_5$), 6.32 (m, 1H, $\eta^6\text{-}C_6H_5$), 5.94 (t, 2H, $J_{H-H}$ = 6.0 Hz, $\eta^6\text{-}C_6H_5$), 5.26 (d, 2H, $J_{H-H}$ = 5.4 Hz, $\eta^6\text{-}C_6H_5$), 4.13 (sept, 1H, $J_{H-H}$ = 6.6 Hz, $NCH(CH_3)_2$), 3.87 (sept, 1H, $J_{H-H}$ = 6.9 Hz, $NCH(CH_3)_2$), 1.68 (d, 6H, $J_{H-H}$ = 6.9 Hz, $NCH(CH_3)_2$), 1.29 (d, 6H, $J_{H-H}$ = 6.6 Hz, $NCH(CH_3)_2$) ppm. $^{13}C\{^1H\}$ NMR (75.5 MHz, $CD_2Cl_2$): $\delta$ 164.8 (d, $J_{C-P}$ = 16.7 Hz, C(Ph)=N), 135.8 (d, $J_{CP}$ = 59.8 Hz, $C_6H_5$), 131.8 (d, $J_{C-P}$ = 10.1 Hz, $C_6H_5$), 130.1 (d, $J_{C-P}$ = 2.8 Hz, $C_6H_5$), 127.6 (d, $J_{C-P}$ = 11.0 Hz, $C_6H_5$), 122.2 (d, $J_{C-P}$ = 6.4 Hz, $\eta^6\text{-}C_6H_5$), 95.7 (d, $J_{C-P}$ = 3.8 Hz, $\eta^6\text{-}C_6H_5$), 91.9 (d, $J_{C-P}$ = 14.3 Hz, $\eta^6\text{-}C_6H_5$), 75.0 (s, $\eta^6\text{-}C_6H_5$), 55.8 (s, $NCH(CH_3)_2$), 48.1 (s, $NCH(CH_3)_2$), 20.3 (s, $NCH(CH_3)_2$), 20.0 (s, $NCH(CH_3)_2$) ppm. $^{31}P\{^1H\}$ NMR (121.5 MHz, $CD_2Cl_2$): $\delta$ 75.9 ppm. DCI MS ($CH_4$, positive mode): $m/z$ 560 $[M]^+$, 525 $[M - Cl]^+$. IR (KBr): $\nu$ 3057 (w), 2979 (w), 2934 (w), 1576 (m), 1558 (s), 1347 (m), 1034 (m), 699 (m), 539 (m) $cm^{-1}$. Crystal data: see Supporting Information.

**9b.** Mp: 149−151 °C. $^1H$ NMR (300.1 MHz, $CD_2Cl_2$): $\delta$ 6.28 (td, $J_{H-H}$ = 6.0 Hz and $J_{H-P}$ = 1.2 Hz, 1H, $\eta^6\text{-}C_6H_5$), 5.87 (t, $J_{H-H}$ = 5.8 Hz, 2H, $\eta^6\text{-}C_6H_5$), 5.03 (d, $J_{H-H}$ = 5.6 Hz, 2H, $\eta^6\text{-}C_6H_5$), 3.92 (sept, $J_{H-H}$ = 6.6 Hz, 1H, $NCH(CH_3)_2$), 3.71 (sept, $J_{H-H}$ = 7.0 Hz, 1H, $NCH(CH_3)_2$), 2.49 (sept d, $J_{H-H}$ = 7.0 Hz and $J_{H-P}$ = 9.2 Hz, 2H, $PCH(CH_3)_2$), 1.57 (d, $J_{H-H}$ = 7.0 Hz, 6H, $NCH(CH_3)_2$), 1.29 (dd, $J_{H-H}$ = 6.9 Hz and $J_{H-P}$ = 14.7 Hz, 6H, $PCH(CH_3)_2$), 1.21 (dd, $J_{H-H}$ = 6.6 Hz and $J_{H-P}$ = 10.0 Hz, 6H, $PCH(CH_3)_2$), 1.22 (d, $J_{H-H}$ = 6.6 Hz, 6H, $NCH(CH_3)_2$) ppm. $^{13}C\{^1H\}$ NMR (50.3 MHz, $CD_2Cl_2$): $\delta$ 164.9 (d, $^2J_{CP}$ = 12.6 Hz, C(Ph)=N), 125.4 (d, $J_{CP}$ = 6.0 Hz, $\eta^6\text{-}C_6H_5$), 98.4 (d, $J_{C-P}$ = 2.5 Hz, $\eta^6\text{-}C_6H_5$), 89.3 (d, $J_{C-P}$ = 13.6 Hz, $\eta^6\text{-}C_6H_5$), 69.9 (s, $\eta^6\text{-}C_6H_5$), 55.9 (s, $NCH(CH_3)_2$), 48.2 (s, $NCH(CH_3)_2$), 28.5 (d, $J_{C-P}$ = 32.3 Hz, $PCH(CH_3)_2$), 21.0 (s, $NCH(CH_3)_2$), 20.2 (s, $NCH(CH_3)_2$), 17.2 (d, $J_{C-P}$ = 25.6 Hz, $PCH(CH_3)_2$) ppm. $^{31}P\{^1H\}$ NMR (121.5 MHz, $CD_2Cl_2$): $\delta$ 113.5 ppm. DCI MS ($CH_4$, positive mode): $m/z$ 492 $[M]^+$, 457 $[M - Cl]^+$. IR (KBr): $\nu$ 3048 (w), 2957 (w), 1566 (s), 1559 (s), 1371 (w), 1345 (w), 1039 (w) $cm^{-1}$. Crystal data: see Supporting Information.

**Synthesis of Complex 11.** A solution of $[(p\text{-cymene})RuCl_2]_2$ (106 mg, 0.17 mmol) in 7 mL of dichloromethane was slowly added to a solution of $i\text{-}Pr_2N{-}C(H){=}N{-}PPh_2$ (**10**) (128 mg, 0.41 mmol) in 3 mL of dichloromethane at room temperature. The reaction mixture was allowed to stir for 3 h, the solvent was removed, and the orange solid was washed with pentane (3 × 10 mL) and dried under vacuum to give 87% (183 mg) yield of **11**. Suitable crystals were obtained from a saturated dichloromethane solution at 4 °C. Mp: 104−106 °C (dec). $^1H$ NMR (200.1 MHz, $CDCl_3$): $\delta$ 8.05 (d, $J_{H-P}$ = 22.5 Hz, 1H, C(H)=N), 7.95−7.85 (m, 4H, $C_6H_5$), 7.36−7.29 (m, 6H, $C_6H_5$), 5.09 (br s, 4H, $C_6H_{4(p\text{-cymene})}$), 4.81 (sept, $J_{H-H}$ = 6.8 Hz, 1H, $NCH(CH_3)_2$), 3.48 (sept, $J_{H-H}$ = 6.8 Hz, 1H, $NCH(CH_3)_2$), 2.69 (sept, $J_{H-H}$ = 6.9 Hz, 1H, $CH(CH_3)_{2(p\text{-cymene})}$), 1.82 (s, 3H, $CH_{3(p\text{-cymene})}$), 1.23 (d, $J_{H-H}$ = 6.8 Hz, 6H, $NCH(CH_3)_2$), 1.11 (d, $J_{H-H}$ = 6.8 Hz, 6H, $NCH(CH_3)_2$), 1.02 (d, $J_{H-H}$ = 6.9 Hz, 6H, $CH(CH_3)_{2(p\text{-cymene})}$) ppm. $^{13}C\{^1H\}$ NMR (50.3 MHz, $CDCl_3$): $\delta$ 158.5 (d, $J_{C-P}$ = 8.6 Hz, C(H)=N), 139.2 (d, $J_{C-P}$ = 52.3 Hz, $C_6H_5$), 132.8 (d, $J_{C-P}$ = 10.1 Hz, $C_6H_5$), 129.5 (d, $J_{C-P}$ = 2.2 Hz, $C_6H_5$), 127.4 (d, $J_{C-P}$ = 10.1 Hz, $C_6H_5$), 122.6 (d, $J_{C-P}$ = 51.1 Hz, $C_6H_5$), 108.9 (s, $C_6H_{4(p\text{-cymene})}$), 94.1 (s, $C_6H_{4(p\text{-cymene})}$), 90.4 (d, $J_{C-P}$ = 4.2 Hz, $C_6H_{4(p\text{-cymene})}$), 86.2 (d, $J_{C-P}$ = 5.8 Hz, $C_6H_{4(p\text{-cymene})}$), 46.6 (s, $NCH(CH_3)_2$), 44.8 (s, $NCH(CH_3)_2$), 30.0 (s, $CH(CH_3)_{2(p\text{-cymene})}$), 23.8 (s, $NCH(CH_3)_2$), 21.8 (s, $CH(CH_3)_{2(p\text{-cymene})}$), 19.9 (s, $NCH(CH_3)_2$), 17.5 (s, $CH_{3(p\text{-cymene})}$) ppm. $^{31}P\{^1H\}$ NMR (81.0 MHz, $CDCl_3$): $\delta$ 58.2 ppm. DCI MS ($CH_4$, positive mode): $m/z$ 618 $[M]^+$, 583 $[M - Cl]^+$. IR (KBr): $\nu$ 3055 (w), 2973 (m), 2926 (w), 2870 (w), 2360 (w), 2341 (w), 1594 (s), 1569 (w), 1434 (m), 1403 (m), 1358 (m), 1295 (m), 1205 (m), 1103 (m), 888 (m), 835 (m), 703 (m), 697 (m), 527 (m) $cm^{-1}$. Crystal data: see Supporting Information.

## Computational Details

Calculations were performed with the Gaussian 03 suite of programs,[27] using the density functional method.[28] The hybrid exchange functional B3LYP set was used. B3LYP[29] is a three-parameter functional developed by Becke that combines the Becke gradient-corrected exchange functional and the Lee−Yang−Parr and Vosko−Wilk−Nusair correlation functionals with part of the exact HF exchange energy. All Gaussian calculations were done in combination with the 6-31G** basis set for C, P, N, Cl, and H (all atoms were augmented with a

(27) Frisch, M. J.; Trucks, G. W.; Schlegel, H. B.; Scuseria, G. E.; Robb, M. A.; Cheeseman, J. R.; Montgomery, J. A.; Vreven, T., Jr.; Kudin, K. N.; Burant, J. C.; Millam, J. M.; Iyengar, S. S.; Tomasi, J.; Barone, V.; Mennucci, B.; Cossi, M.; Scalmani, G.; Rega, N.; Petersson, G. A.; Nakatsuji, H.; Hada, M.; Ehara, M.; Toyota, R.; Fukuda, J.; Hasegawa, M.; Ishida, T.; Nakajima, Y.; Honda, O.; Kitao, H.; Nakai, M. X.; Klene, X.; Li, K.; Knox, J. E.; Hratchian, H. P.; Cross, J. B.; Adamo, C.; Jaramillo, J.; Gomperts, R.; Stratmann, R. E.; Yazyev, O.; Austin, A. J.; Cammi, R.; Pomelli, C.; Ochterski, J. W.; Ayala, P. Y.; Morokuma, K.; Voth, G. A.; Salvador, P.; Dannenberg, J. J.; Zakrzewski, V. G.; Dapprich, S.; Daniels, A. D.; Strain, M. C.; Farkas, D. K.; Malick, A. D.; Rabuck, K.; Raghavachari, J. B.; Foresman, J. V.; Ortiz, Q.; Cui, A. G.; Baboul, S.; Clifford, O.; Cioslowski, J.; Stefanov, B. B.; Liu, G.; Liashenko, A.; Piskorz, P.; Komaromi, I.; Martin, R. L.; Fox, D. J.; Keith, T.; Al-Laham, M. A.; Peng, C. Y.; Nanayakkara, A.; Challacombe, M.; Gill, P. M. W.; Johnson, B.; Chen, W.; Wong, M. W.; Gonzalez, C.; Pople, J. A. *Gaussian 03, Revision D-02*; Gaussian, Inc.: Pittsburgh, PA, 2003.

(28) Parr R. G.; Yang W. *Functional Theory of Atoms and Molecules*; Breslow, R., Goodenough, J. B., Eds.; Oxford University Press: New York, 1989.

(29) (a) Becke, A. D. *Phys. Rev. A* **1988**, *38*, 3098. (b) Becke, A. D. *J. Chem. Phys.* **1993**, *98*, 5648. (c) Lee, C.; Yang, W.; Parr, R. G. *Phys. Rev. B* **1988**, *37*, 785.

single set of polarization functions) and the set RECP (relativistic effective core potential) SDD[30] for Ru. SDD is the combination of the Huzinaga−Dunning double-ζ basis set on lighter elements with the Stuttgart−Dresden basis set RECP on transition metals. Geometry optimizations were carried out without any symmetry restrictions; the nature of the extrema (minimum) was verified with analytical frequency calculations. All Gibbs free energies have been zero-point energy (ZPE) and temperature corrected using unscaled density functional frequencies. Natural bond orbital (NBO 3.1 implemented in Gaussian 03)[31] analysis was used to determine the stabilizing interactions and the hybridization of the atoms involved in the $\sigma_{PN}$ and $\sigma_{CN}$ bonds and in the imino nitrogen lone pair. Molecular orbitals have been plotted with the Molekel package.[32]

**Acknowledgment.** We thank the CNRS for financial support and the European Community (Fond Social Européen) for a postdoctoral fellowship to D.A. We thank the Institut du Developement de Ressources en Informatique Scientifique administered by the CNRS for the calculation facilities.

**Supporting Information Available:** General experimental information, crystallographic data (including cif files) for compounds **2**, **5**, **7**−**9**, and **11** (CCDC 689855−689857 and CCDC 717807−717812), and theoretical data (Z-matrices and NBO results). This material is available free of charge via the Internet at http://pubs.acs.org.

(30) (a) Dolg, M. *Modern Methods and Algorithm of Quantum Chemistry, Vol. 1*; Grotendorst, J., Ed.; John von Neuman Institute for Computing: Jülich (Germany), 2000; p 479. (b) Dolg, M.; Wedig, U.; Stoll, H.; Preuss, H. *J. Chem. Phys.* **1987**, *86*, 866. (c) Andrae, D.; Häussermann, U.; Dolg, M.; Stoll, H.; Preuss, H. *Theor. Chim. Acta* **1990**, *77*, 123.

(31) (a) Reed, A. E.; Curtiss, L. A.; Weinhold, F. *Chem. Rev.* **1988**, *88*, 899. (b) Foster, J. P.; Weinhold, F. *J. Am. Chem. Soc.* **1980**, *102*, 7211.

(32) (a) Flükiger, P.; Lüthi, H. P.; Portmann, S.; Weber, J. *Molekel 4.3*; Swiss Center for Scientific Computing: Manno, Switzerland, 2000−2002. (b) Portmann, S.; Lüthi, H. P. Molekel: An Interactive Molecular Graphics Tool. *Chimia* **2000**, *54*, 766.